ISSN 1846-6168 (Print), ISSN 1848-5588 (Online)
https://doi.org/10.31803/tg-20240919083722

Original scientific paper
Received: 2024-09-19, Accepted: 2024-11-12

Determination of Thermal Characteristics of Fe-C Cast Iron Using Hot Disk Method

Dalibor Videršćak*, Zdravko Schauperl, Sanja Šolić, Bojan Milovanović, Ivan Stanković, Mario Šercer

Abstract: This paper explores the influence of graphite shape, type, and dimensions on the thermal characteristics of Fe-C cast iron. Test samples were prepared from blocks of grey and nodular cast iron, specifically examining castings with D and A types of graphite as well as nodular graphite in a ferrite matrix. To analyze the effect of surface texture, sample surfaces were prepared with varying parameters of surface roughness, achieving values of 0.5 μm for polished and 12.6 μm for unpolished surfaces. Thermal characteristics, including thermal conductivity and effusivity, were evaluated using unsteady hot disk methods, with water as the contact agent, to simulate practical thermal conditions. Additionally, the microstructure of each sample was analyzed using optical microscopy. Results indicate that graphite content, type, shape, and surface roughness collectively have the most significant impact on the thermal properties of cast iron. This study's findings provide valuable insights into optimizing cast iron for applications requiring efficient thermal management and highlight the importance of graphite morphology and surface finish in enhancing thermal performance.

Keywords: graphite; grey cast iron; hot disk method; nodular cast iron; thermal conductivity; thermal effusivity

1 INTRODUCTION

According to recent data, the global production of grey cast iron reached approximately 31 million tons in 2023, and it is projected to increase to 41 million tons by 2034, with an average annual growth rate (CAGR) of 2,5%. This growth is attributed to its extensive use in the automotive, construction, and industrial consumer goods sectors [1].

Regarding nodular (ductile) cast iron, global production continues to expand due to its widespread application in industries such as automotive and heavy machinery [1, 2]. In Europe, for example, in 2021, nodular cast iron accounted for approximately 43.5% of the total production of ferrous castings, while grey cast iron represented 49.3% (CAEF - The European Foundry Association and Future Market Insights). These figures indicate a continuous increase in the production of both types of cast iron, underscoring their critical roles in various industrial sectors and infrastructure projects [3, 4].

Thermal and mechanical properties of Fe-C cast iron primarily depend on its structure, concretely amount and the form of graphite [5]. The quantity of extracted graphite within the matrix of Fe-C cast iron directly depends on the equivalent of graphite (CE): $CE = \%C + 1/3 \times (\%Si + \%P)$ [4]. This indicates that the higher value of the coefficient of CE generally results in a higher amount of extracted graphite. At the same time, there will be an increase of values of thermal characteristics, while a decrease of values of mechanical characteristics [6, 7]. Besides chemical composition, type of extracted graphite mostly depends on the method of cast iron production [8]. Based on the reasons above ASTM suggests a standard for the classification of graphite according to ASTM A247-47 and 67 and upgrades it to the International Standards Organization ISO Recommendation 9, according to which graphite differs according to its shape, size and layout of graphite structure [9–11]. Because there are many kinds of grey and nodular casts iron which differ chemically, by phases in the matrix (ferrite, perlite, bainit, cementit etc.) and their quantity content, according to the shape and dimensions of graphite, and likewise, it is important to note that there are no standard samples of Fe-C cast iron [4]. For this reason, this paper shows the results of the characterization according to the structure, chemical composition and thermal characteristics of these types of cast iron, as well as a comparison of the thermal characteristics of the sample, depending on the roughness of the surface tested by the hot disk method [4, 8].

Recent studies have emphasized the importance of these thermal and mechanical properties in various high-stress applications, such as brake components, which are subject to significant thermal loads. Dubale's (2019) doctoral research, for instance, analyzed the thermo-mechanical behavior of disc brake rotors, highlighting the critical role of thermal conductivity and structural resilience in components exposed to friction-induced heating. Similarly [12] Venugopal et al. (2023) examined grey cast iron under electrical discharge machining (EDM) processes, emphasizing the relationship between thermal management and wear resistance in high-temperature environments. These findings underscore the need to accurately characterize cast iron's thermal properties to predict its behavior in thermally demanding applications.

Moreover, the tribological properties of Fe-C cast iron also play a significant role in component durability, as highlighted by [13] Skulić & Bukvić (2016), who studied the impact of surface roughness on piston-cylinder sets in internal combustion engines. Their findings demonstrate how surface roughness and graphite morphology influence both thermal conductivity and wear resistance in mechanical assemblies. This underscores the necessity of assessing thermal behavior in cast iron with varying graphite shapes and roughness levels to optimize material performance in practical applications.

Pretested samples of grey cast iron containing A and D type flake (lamellar) graphite in a ferritic matrix showed that they give cast iron a fragile structure of low ductility, relatively low tensile strength and high compressive strength and relatively high thermal conductivity. In pretested samples of nodular cast iron containing graphite in the form of nodules in a ferrite matrix it is shown that they give cast iron a relatively tough structure with good mechanical

characteristics and lower thermal conductivity compared to the grey cast iron with type A and D graphite [11, 14-16]. It is important to note that preliminary tests show that reducing the amount of graphite in grey cast iron increases the tensile strength and fatigue strength, respectively the values of mechanical properties [5, 15], while the values of thermal characteristics decrease [18].

Grey and nodular graphite iron are primarily used in at manufacture of brake discs, heating plates on ovens, molds for casting glass, gears, motor shafts, cover sliding bearings, pump impellers, pistons and gear motors, etc. [2, 12]. As most of these elements in practice are extremely thermally loaded, it is important to know the thermal conductivity of grey and nodular cast iron castings to be able to predict the thermodynamic processes in the machine elements [10, 17].

Given the diverse types of grey and nodular cast iron, each with unique chemical compositions, matrix phases (e.g., ferrite, pearlite, bainite), and graphite configurations, this study aims to provide a comprehensive characterization of these materials. Specifically, it examines the thermal properties of cast iron samples with A and D type graphite in a ferritic matrix, as well as nodular cast iron with graphite nodules. By investigating surface roughness through hot disk testing, this study evaluates how surface texture and graphite morphology impact thermal conductivity. The findings from these analyses are essential for designing cast iron components in high-temperature applications, such as brake discs, heating elements, and engine parts, where understanding thermodynamic processes is crucial.

2 MATERIALS AND METHODS

In the experimental part of the study three samples of Fe-C cast iron of different surface roughness with different forms of graphite were tested, all three in the ferrite matrix, Fig. 1.

Sample 9D is a type of grey cast iron with a type D flake graphite in a ferritic matrix, and an average volume fraction of 8.90% of graphite in the alloy in the solid state. Sample 1A is grey cast iron with a type A flake graphite in ferritic matrix and an average volume fraction of 10.50% graphite within the alloy in the solid state. Type A graphite, with a uniform appearance and shape within a grey cast iron, occurs because of moderate cooling, while type D graphite occurs because of deeper subcooling during the production process [8, 14, 18]. In laboratory research, it was obtained that these two samples of grey cast iron with different types of graphite have the same chemical composition and hardness but have different appearance and shape of graphite sheets which is achieved by controlled cooling of samples during the casting process. Sample 13 is a nodular cast iron with graphite nodular type ferrite in the matrix, and the average volume fraction of 6.70% in the alloy in the solid state. Nodular graphite inside cast iron forms its nodular form in melt during the manufacturing process and is characterized by that it is of proper spherical shape [1, 17, 19]. A quantity content of graphite or a volume percentage of graphite within the three Fe-C casts is determined according to ASTM E 562-11 [22].

Brinell hardness value of 202 HBW10/3000 was obtained for samples 9D and 1A, and for sample 13 the value of obtained hardness was 152 HBW10/3000, both according to HRN EN ISO 6506-1:2014 [23].

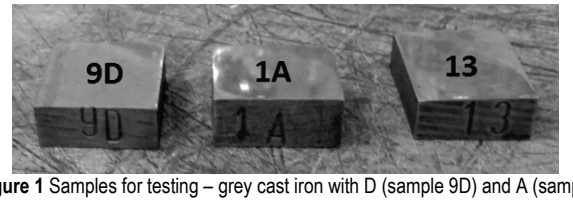

Figure 1 Samples for testing – grey cast iron with D (sample 9D) and A (sample 1A) type flake (lamellar) graphite, and nodular cast iron with graphite in a form of nodules (sample 13)

Table 1 Percentage of chemical elements in three Fe-C test samples

Grey cast iron with D type flake graphite – sample 9D (%)										
C	Si	Mn	P	S	Cr	Ni	Mo	V	Ti	Fe
3.21	2.41	0.59	0.162	0.044	0.00	0.10	0.02	0.06	0.01	Rest.
Grey cast iron with A type flake graphite – sample 1A (%)										
C	Si	Mn	P	S	Cr	Ni	Mo	V	Ti	Fe
3.21	2.41	0.59	0.162	0.044	0.00	0.10	0.02	0.06	0.01	Rest.
Nodular cast iron with graphite in the form of nodules – sample 13 (%)										
C	Si	Mn	P	S	Cr	Ni	Mo	V	Ti	Fe
3.55	2.50	0.66	0.051	0.007	0.003	0.003	0.008	0.03	0.126	Rest.

Since there have been two test surfaces with different profile roughness parameters produced in each group of samples, it was necessary to determine their different profile roughness parameters. The measurement has been carried out by contact method in electronic - mechanical device stylus Perthometer C5D. The Perthometer C5D specializes in measuring surface roughness parameters, such as *Ra* (average roughness) and *Rz* (mean peak-to-valley height), with high precision, typically ± 0.1 μm. However, it requires stable conditions as environmental vibrations and reflective surfaces can affect accuracy. Different profile roughness parameters for the non-polished side of samples is *Ra* – 12.6 ± 0.1 μm, while for the polished side of the sample is as follows: *Ra* – 0.5 ± 0.1 μm. Roughness levels were consistent across all tested samples. This consistency in roughness values was essential for accurately assessing the impact of surface finish on thermal conductivity and effusivity across different graphite-containing cast iron samples. Broad range of surface roughness values was chosen (0.5 μm for polished and 12.6 μm for unpolished) to comprehensively investigate the impact of surface finish on thermal characteristics. This range allows a detailed analysis of impact surface roughness affect thermal conductivity and effusivity, offering insights

applicable to real-world applications where surface roughness varies.

The chemical composition of all three samples is determined by using a Leco GDS500 A that is based on the method of Glow Discharge Atomic Emission Spectrometry (AES) [24], and the percentage of resulting chemical elements of all three casts is shown in Tab. 1.

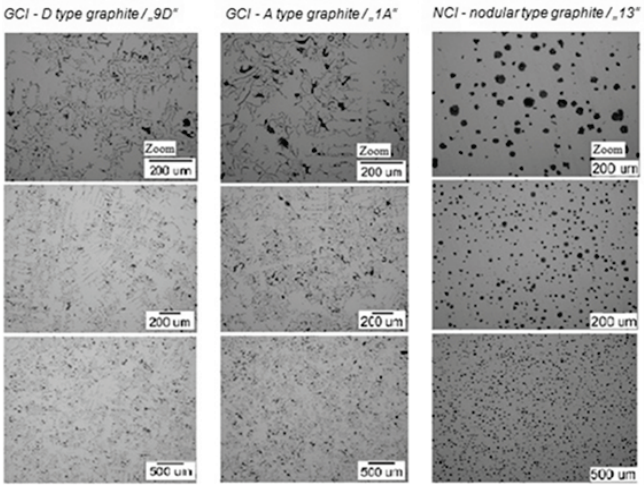

Figure 2 Microstructures of test samples; light microscope

2.1 Microstructure Analysis

A microstructure of the samples was analyzed. The samples were prepared in such a way that they were ground, polished and pitted. Grinding was conducted with abrasive grit paper P 4000, polishing was conducted by diamond paste, while the etching was performed in Nital, a 3% solution of nitric acid in ethyl alcohol. Analysis of the microstructure was conducted on a light microscope Olympus GX51 Analyzer. The Olympus GX51 Analyzer is a metallurgical microscope offering magnification up to 1000×, designed for detailed examination of material microstructures, including grain size and phase distribution. Although highly capable, it requires precise calibration and smooth sample surfaces for accurate analysis, with limitations on rough or highly reflective samples. The resulting microstructures of the three test samples are shown in Fig. 2.

2.2 Testing Method

Testing was carried out by a device Mathis TCi. The Mathis TCi instrument measures thermal properties, specifically thermal conductivity, diffusivity, and effusivity, using the modified transient plane source (MTPS) technique. It operates with ± 5% accuracy across a range of 0.03 to 30 W/mK, suitable for diverse materials from insulators to conductors. Accurate results with the Mathis TCi depend on smooth sample contact, as inconsistencies in surface quality may impact measurements. Together, these devices provide a robust profile of surface, structural, and thermal properties essential for in-depth material analysis. This kind of device is based on a non-stationary method of testing thermal performance of a material which is referred to as a hot disk method. The device consists of a sensor, a control unit and a computer program that manages and collects data measurements [24]. This type of device directly measures thermal conductivity and thermal effusivity as well as thermal diffusivity and heat capacity [25]. The method is based on passing a one-dimensional heat flow from the sensor to the sample so that the sensor is located within several concentrically wrapped rings, spirals, or 10-micron thick wires made of platinum, which are a constant source of heat transferred to the upper glass surface of the sensor, and through which a one-dimensional heat flow travels towards the sample [26].

The spiral is made of platinum because platinum is a material that has the feature of excellent linear stretching and contraction at a wide range of temperatures. The main components of the device are shown in Fig. 3.

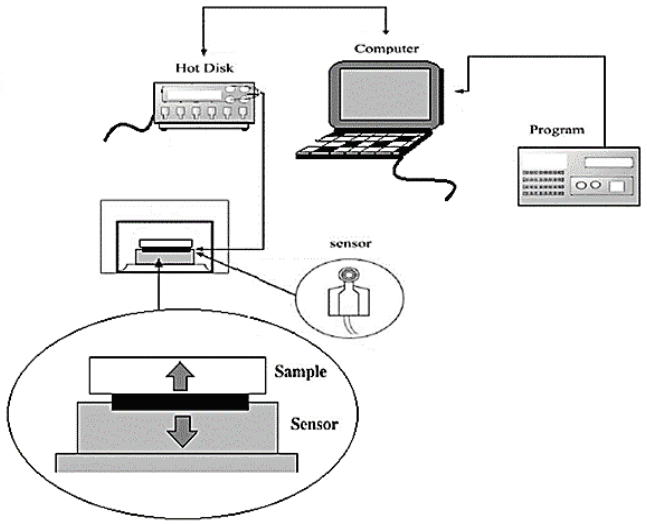

Figure 3 Components of the device and a diagram of the device for testing thermal characteristics based on the hot disk method

The device assumes a one-dimensional heat flow in the direction of the sensor towards the sample, while at the same time ignoring the thermal resistance of the touch sensor and the sample. With that in mind, a change of contact surface temperature sensor ($x = 0$) is given by the Eq. (1):

$$\Delta T(x=0,\, t) = \frac{1.1284 \cdot G \cdot \sqrt{t}}{e_1 + e_2}, \tag{1}$$

where ΔT (°C) is a temperature change of contact temperature, G (W/m²) a density of heat flow that comes into the sensor, t (sec) time measured from the beginning of the process, e_1 (W√(s/m²K)) is equivalent effusivity of the sensor and e_2 (W√(s/m²K)) is effusivity of the tested sample [26, 25]. Value the change of the contact temperature to equivalent voltage change is converted by the temperature coefficient of resistance TCR. The relation between the sensor resistance and its temperature is determined by the Eq. (2):

$$R(T) = R_0(1 + \alpha \cdot T) = R_0 + AT, \tag{2}$$

where $R(T)$ of the sensor resistance at the temperature T, the sensor resistance R_0 at 0 °C, the sensor temperature T (°C), α the temperature coefficient of resistance (TCR) and A slope of correlation [25, 26]. Applying Ohm's Law to connect Eq. (1) and Eq. (2) yields Eq. (3).

$$\Delta V(t) = \frac{1.1284 \cdot I \cdot A \cdot G \cdot \sqrt{t}}{e_1 + e_2}. \tag{3}$$

Then, the Eq. (3) can be written as Eq. (4):

$$\Delta V(t) = m \cdot \sqrt{t}, \tag{4}$$

where m is the slope of the line that describes the change in voltage with respect to the root of time, according to the value of the Eq. (5):

$$m = \frac{1.1284 \cdot I \cdot A \cdot G}{e_1 + e_2}. \tag{5}$$

The assumption is that in the short period, all parameters on the right side of the Eq. (5) are constant, then the heat effusivity e_2 would be calculated according to the Eq. (6):

$$\frac{1}{m} = M_2 \cdot e_2^2 + M_1 \cdot e_2 + C, \tag{6}$$

where M_1 and M_2 are sensor constants that depend on a type of testing sample and C is a characteristic of the sensor dependent on the temperature T during the testing, the Eq. (7).

$$C = C_0 + C_1 \cdot T + C_2 \cdot T^2, \tag{7}$$

where C_0, C_1 and C_2 are constants of a sensor [25, 26].

Measurement of thermal conductivity λ is based on data collected for obtaining heat effusivity, through the algorithm m^* for calibration and calculation of thermal conductivity. The device uses an iterative process to calibrate the sensor, based on known values of coefficients of thermal conductivity. Thermal conductivity is calculated according to the Eq. (8):

$$\frac{1}{m - m^*} = \alpha \cdot \lambda + z, \tag{8}$$

where α is the slope, and z cutting values on the calibration curve [25, 26]. The formulas used in this paper are derived from a combination of established sources and original derivations tailored to the specific experimental setup. Formulas related to thermal conductivity and effusivity are based on the Mathis TCi Thermal Conductivity Instrument User Manual by Mathis Instruments, Inc., which details the MTPS (Modified Transient Plane Source) method for thermal property measurements. Equations involving thermal resistance and voltage-based calculations are grounded in the principles found in Introduction to Heat Transfer by Incropera and DeWitt, covering fundamental concepts of heat transfer and thermal resistance. Additionally, general equations for thermal conductivity in alloys, particularly Fe-C alloys, are referenced from Materials Science and Engineering: An Introduction by Callister and Rethwisch. Any formulas unique to this study have been specifically derived by the authors to meet the experimental conditions and are indicated as original contributions in the paper.

2.3 Research

In addition to the influence of graphite, the paper also explored the influence of surface roughness on the sample's thermal characteristics.

Table 2 Characteristics of test Fe-C samples

Characteristics	Grey cast iron		Nodular cast iron
Label of cast iron	9D	1A	13
Type of graphite	D graphite	A graphite	Nodules
Percentage of graphite (%)	8.90	10.50	6.70
Dimensions of sample (mm)	10.98/27.87/ 26.05	12.32/27.83/ 23.41	10.72/30.89/ 25.87
Weight of sample (kg)	0.055	0.056	0.059
Density of sample (kg/m³)	6838.14	6959.12	6.892.52
Ambient temperature (°C)	23 ± 2		
Coupling agent	Water		

Three measurements was carried out for each surface sample, each measurement had 10 readings, with each reading lasting 60 seconds. It takes from 0,8 to 5 seconds for the reading and the rest of the 60 seconds during the interval readings serve for a complete cool down of the sample [25]. The test was carried out with water as a coupling agent at a room temperature of 23 ± 2 °C - water is used for testing in temperature ranges from 5 °C to 70 °C [24, 26]. The main characteristics of Fe-C test samples are shown in Tab. 2.

3 RESULTS AND DISCUSSION

Tab. 3 shows the results of mean values of specific heat capacity and thermal diffusivity of test Fe-C samples depending on the surface roughness and the type of graphite.

Table 3 Results of mean values of specific heat capacity and thermal diffusivity of test Fe-C samples

Fe-C samples	Specific heat capacity (J/kg/K)	Thermal diffusivity (m²/s)
Sample 9D - polished side (Ra = 0.5 μm)	166.40	1.25×10^{-4}
Sample 9D - non polished side (Ra = 12.6 μm)	354.96	1.43×10^{-5}
Sample 1A - polished side (Ra = 0.4 μm)	121.72	2.54×10^{-4}
Sample 1A - non polished side (Ra = 12.4 μm)	168.80	1.17×10^{-4}
Sample 13 - polished side (Ra = 0.6 μm)	327.68	1.89×10^{-5}
Sample 13 - non polished side (Ra = 12.5 μm)	378.22	9.94×10^{-6}

Fig. 4 and Fig. 5 show graphs of the results of the thermal conductivity and heat effusivity of the Fe-C samples depending on the surface roughness and type of graphite. Graphs show the minimum, maximum and mean value for each test sample depending on the surface roughness, and its comparison.

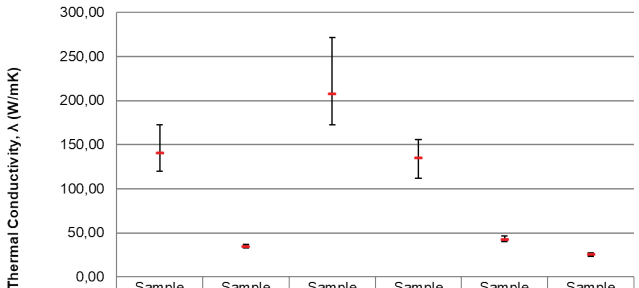

	Sample "9D" - polished side	Sample "9D" - non polished side	Sample "1A" - polished side	Sample "1A" - non polished side	Sample "13" - polished side	Sample "13" - non polished side
Max. value	172,88	36,94	271,33	155,73	46,51	27,59
Min. value	120,14	32,59	172,30	112,22	40,54	23,76
Average value	140,35	34,58	207,78	134,83	42,64	25,91

Figure 4 Results of mean values of thermal conductivity of test Fe-C samples with their minimum and maximum values

Since pure graphite is an anisotropic element having different thermal conductivities depending on the orientation of the crystal lattice, a large deviation of the results is expected [27]. Therefore, it is necessary to analyze the value of standard deviations and coefficients of variation of test samples obtained based on the results of thermal conductivities and thermal effusivities, shown in Tab. 4.

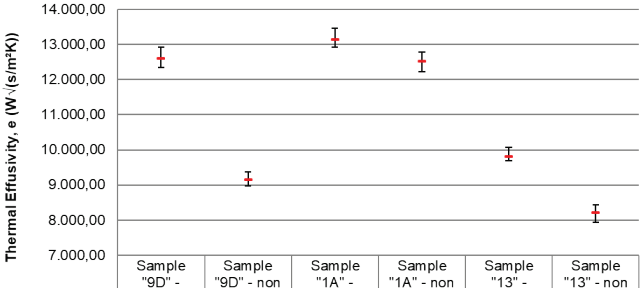

	Sample "9D" - polished side	Sample "9D" - non polished side	Sample "1A" - polished side	Sample "1A" - non polished side	Sample "13" - polished side	Sample "13" - non polished side
Max. value	12.926,51	9.370,53	13.457,85	12.774,61	10.072,29	8.427,10
Min. value	12.344,19	8.971,78	12.921,88	12.217,73	9.682,32	7.931,31
Average value	12.600,96	9.157,47	13.141,34	12.527,98	9.811,55	8.213,93

Figure 5 Results of mean values of thermal effusivity of test Fe-C samples with their minimum and maximum values

Obtained values of standard deviation and coefficient of variation concerning the tested side of the sample are relatively small, which indicates that the average deviation of individual values from the mean value is relatively small, and it shows relatively high uniformity of the results. Tab. 4 shows that sample 13 obtained at least an average deviation of the individual values of the arithmetic mean, indicating a relatively high uniformity of the results. A bit larger average deviation of the individual values from the mean was obtained at sample 9D, but also shows a relatively high uniformity of the obtained results. The largest average deviation of the individual values of arithmetic mean was obtained for sample 1A which tells us that there is a relatively small uniformity of the results obtained, which of course is not desirable. Also, in Tab. 4, a smaller average deviation of the individual values from the mean was obtained with non-polished samples compared to polished samples.

Table 4 Measures of dispersion mean values of thermal conductivity and thermal effusivity of test Fe-C samples

Measures of dispersion mean values of thermal conductivity of Fe-C test samples			
Fe-C samples		Standard deviation, σ	Coefficient of variation, V (%)
Sample 9D	Polished side (Ra = 0.5 μm)	12.88	9.19
	Non polished side (Ra = 12.6 μm)	0.77	2.19
Sample 1A	Polished side (Ra = 0.4 μm)	27.33	12.77
	Non polished side (Ra = 12.4 μm)	10.87	7.88
Sample 13	Polished side (Ra = 0.6 μm)	1.18	2.75
	Non polished side (Ra = 12.5 μm)	0.44	1.68
Measures of dispersion mean values of thermal effusivity of Fe-C test samples			
Fe-C samples		Standard deviation, σ	Coefficient of variation, V (%)
Sample 9D	Polished side (Ra = 0.5 μm)	145.80	1.16
	Non polished side (Ra = 12.6 μm)	69.95	0.76
Sample 1A	Polished side (Ra = 0.4 μm)	149.72	1.14
	Non polished side (Ra = 12.4 μm)	128.49	1.02
Sample 13	Polished side (Ra = 0.6 μm)	82.78	0.84
	Non polished side (Ra = 12.5 μm)	55.95	0.68

The results show a significant difference in thermal conductivity and effusivity depending on the amount, type and distribution of graphite particles and the surface roughness. The greater thermal conductivity of polished samples can be explained by the fact that at non polished side of the sample there is a better chance for at presence of residual air in microcavities at the contact of the sensors and the sample. Because of that, it has an impact on a decrease of read value of thermal conductivity due to the low value of thermal conductivity of air at room temperature, which is λAIR = 0,026 W/mK, in relation to the resulting thermal conductivities of casts [1, 28].

From the obtained results of measurements, it has been shown that thermal conductivity and effusivity of materials depend on the type and quantity of graphite inside the cast at the micro level. It can be seen in Figs. 4-5 that the values of thermal conductivity and effusivity are lowest in nodular cast iron with 6.70% graphite in the form of nodules (sample 13), while in grey cast iron with 8.90% D type flake (lamellar) graphite (sample 9D) they are somewhat higher. The greatest values of thermal conductivity and effusivity were obtained by testing a sample of grey cast iron with 10.50% A type flake (lamellar) graphite (sample 1A). The above shows the fact that the thermal conductivity of tested iron cast samples

increases with the amount of graphite in test samples. The same is true for the values of thermal effusivities, specific heat capacities and thermal diffusivities. The thermal conductivity of iron is $\lambda_{IRON} \approx 70$ to 80 W/mK, while the thermal conductivity of graphite differs whether it is measured parallelly ($\lambda_{GRAPHITE,} \parallel \approx 25$ to 274 W/mK) or perpendicularly to the basal plane ($\lambda_{GRAPHITE,} \perp \approx 10$ W/mK) [26, 27]. Hence the conclusion is that thermal conductivity of test casts depends on the amount of graphite and the orientation of the basal plane of graphite relative to the position one-dimensional heat flow sensor device for testing. It tells us that a higher value of thermal conductivity was obtained in samples with a higher amount of graphite where one-dimensional heat flow traveled parallelly to the basal graphite plane, and vice versa. Because of that, in anisotropic materials it is necessary, by hot disk method, to measure thermal conductivity in several orientations relative to the test sample to obtain a more realistic result.

4 CONCLUSION

In this paper, the results of testing thermal conductivity and effusivity are shown on samples of grey cast iron with A and D type flake graphite in a ferritic matrix and nodular cast iron with nodular graphite in a ferritic matrix using the non-stationary method of the hot disk. The method of hot disk is a fast and simple, but sensitive method that is most often used in quality control in production and development of materials.

The test concluded that the value of the thermal conductivity and effusivity of tested samples mostly depends on the roughness of the surface on which the testing is being conducted and, on the form, type, layout, orientation and the amount of graphite in cast iron. The results show a higher value of thermal conductivity and effusivity tested on the polished side of the sample. Also, it has been shown that for the samples with a higher quantity content of graphite and denser layout of graphite granules at the microstructural level higher values of thermal conductivity and effusivity are obtained.

In the end, by statistical measures of dispersion, it is proved that a relatively low deviation of the individual values is obtained from the arithmetic mean of the same, which shows a relatively high consistency of the results obtained by this method of testing.

The results of this study indicate a significant influence of graphite type, shape, and distribution, along with surface roughness, on the thermal conductivity and effusivity of Fe-C cast iron. This lays a strong foundation for future research into optimizing thermal and mechanical characteristics for industrial applications. Expanding this work, further studies could investigate Fe-C cast iron with varied carbon percentages and explore additional graphite morphologies, as these factors could yield new insights into enhancing both thermal management and structural resilience of cast iron components.

Future experiments could also involve testing under diverse environmental conditions, such as higher or variable temperatures, to simulate real-world applications more accurately. Exploring alternative alloying elements or incorporating nanoparticles within the Fe-C matrix could further advance the material's thermal properties. These additional conditions would not only support broader industrial uses, such as in brake discs and engine components but might also reduce operational and maintenance costs by extending the material's lifespan in thermal applications. Ultimately, these studies would help refine Fe-C cast iron's applicability in mechanical constructs requiring specific thermal characteristics, such as cooling systems or high-wear components, while promoting cost efficiency through improved material performance.

Acknowledgement

This research was supported by the project KK.01.1.1.07.0013 - Innovative Ti-Mg dental implants for the world market.

5 REFERENCES

[1] Zhou, X., Li, Y., Huang, X., & Wu, W. (2023). Recent Advances in Thermal Conductivity of Cast Irons: A Review. *Materials Science and Engineering: A*, 870, 144664. https://doi.org/10.1016/j.msea.2023.144664

[2] Xiao, Y., Liu, J., Wang, Z., & Sun, Q. (2020). Study on the Thermal Conductivity of Compacted Graphite Cast Iron and Its Application in Automotive Brake Discs. *Automotive Engineering, 42*(5). 495-502. https://doi.org/10.3969/j.issn.1671-7277.2020.05.005

[3] Staff report MC. (2014). 48th Census of World Casting Production. Steady Growth in Global Output. Modern Casting. 17-21.

[4] Zhang, Y., Wei, X., Sun, J., & Liu, Y. (2021). Thermal Conductivity and Microstructure of Cast Irons Under Various Heat Treatment Conditions. *Materials Characterization*, 180, 111354. https://doi.org/10.1016/j.matchar.2021.111354

[5] Wang, J., Zhang, L., & Liu, X. (2022). Effects of Graphite Morphology on the Mechanical and Thermal Properties of Gray Cast Iron. *Journal of Materials Science, 57*(10), 5123-5136. https://doi.org/10.1007/s10853-022-07067-9

[6] Hecht, R. L., Dinwiddie, R., Porter, W. D., & Wang H. (1996). Thermal Transport Properties of Grey Cast Irons. *SAE transaction, 105*, 1699-1705. https://doi.org/10.4271/962126

[7] Bockus, S. (2006). A study of the microstructure and mechanical properties of continuously cast iron products. *METABK, 45*(4), 287-290.

[8] Gomez, M., Dominguez, F., & Ortega, A. (2021). Evaluation of Graphite Nodularity and Its Effects on the Thermal Properties of Nodular Cast Irons. *Journal of Engineering Materials and Technology, 143*(3), 31012. https://doi.org/10.1115/1.4049351

[9] Sjögren, T. (2007). Influences of the Graphite Phase on Elastic and Plastic Deformation Behaviour of Cast Irons. https://doi.org/10.1007/s11661-007-9115-8

[10] Angus, H. T. (1976). *Cast Iron: Physical and Engineering Properties*. Second. 1-33. https://doi.org/10.1016/B978-0-408-70933-0.50006-2

[11] Prakash, P., Mytri, V. D., & Hiremath, P. S. (2011). Digital Microstructure Analysis System for Testing and Quantifying the Ductile Cast Iron. *International Journal of Computer Applications, 19*(3).

[12] Venugopal, P., Saravanan, K. G., & Thanigaivelan, R. (2023).

Performance Analysis of Edm on Grey Cast Iron Using Rsm and Topsis Method. *Applied Engineering Letters, 8*(1), 10-16. https://doi.org/10.18485/aeletters.2023.8.1.2

[13] Skulić, A., & Bukvić, M. (2016). Tribological properties of piston-cylinder set in internal combustion engines. *Applied Engineering Letters, 1*(1), 29-33.

[14] Shifani Madtha, L., & Narendra Babu, B. R. (2013). Experimental Behavioural Study of Ductil Cast Iron Microstructure and Its Mechanical Properties. International *Journal of Engineering Research and Applications (IJERA), 3*(3), 1470-1475.

[15] Samuelsson, D. P. B. (2011). Analysis of microstructural strain-fields in grey cast iron. Diploma work No. 47/2011. https://odr.chalmers.se/server/api/core/bitstreams/b8adf42c-9daf-4045-a88f-5dfb832a47ce/content

[16] Martinez, F., Gonzalez, A., & Sanchez, L. (2021). Thermal Conductivity Measurement of Graphitic Cast Irons Using Hot Disk Method. *Journal of Thermal Analysis and Calorimetry, 144*(3), 1747-1758. https://doi.org/10.1007/s10973-020-09619-3

[17] Collini, L., Nicoletto, G., & Konečná, R. (2008). Microstructure and mechanical properties of pearlitic gray cast iron. *Materials Science and Engineering: A*, 488, 529-539. https://doi.org/10.1016/j.msea.2007.11.070

[18] Lee, J., Kim, S., & Park, H. (2023). Analysis of Microstructural Effects on Thermal Conductivity in High-Alloy Cast Irons. *Materials Today: Proceedings, 74*, 208-216. https://doi.org/10.1016/j.matpr.2023.07.017

[19] Rodriguez, E., Fernandez, J., & Ortega, R. (2020). Influence of Heat Treatment on the Thermal Conductivity of Gray Cast Iron. *Materials Research Express, 7*(11), 115501. https://doi.org/10.1088/2053-1591/abc544

[20] Ohser, J., Sandau, K., Stets, W., & Gerber, W. (2003). Image Analytical Characterization of Graphite in Grey Cast Iron and Classification on Lamellar Arrangement. *Practical Metallography, 40*(9), 454-473. https://doi.org/10.1515/pm-2003-400906

[21] Moumeni, E. (2013). *Solidification of cast iron - A study on the effect of microalloy elements on cast iron*.

[22] ASTM E 562 - 01. (2011). *Standard Test Method for Determining Volume Fraction by Systematic Manual Point Count*. West Conshohocken, PA.

[23] EN ISO 6506-1:2014. Metallic materials -- Brinell hardness test -- Part 1: Test method.

[24] Maul, C. L. (2008). *Glow Discharge Atomic Emission Spectrometry - The Methodology, Calibration and Analytical Performance for Bulk and Quantitative Depth Profile Analysis*.

[25] Mikulić, D. & Milovanović, B. (2010). TCi system for non-destructive determination of thermal properties of materials. In: *10th European Conference on Non Destructive Testing*. Publishing house Spektr, 256-266.

[26] Instruments M. Mathis TCi User Manual. c-Therm Technologies Ltd., 21 Alison Blvd., Fredericton, Canada; 2008.

[27] Velichko, A. (2008). Quantitative 3D Characterization of Graphite Morphologies in Cast Iron using FIB Microstructure Tomography. Chemie, Pharmazie, Bio- und Werkstoffwissenschaften der Universität des Saarlandes, Saarbrücken, Germany. https://doi.org/10.22028/D291-22506

[28] McQuillan, F. J., Culham, J. R. & Yovanovich, M. M. (1984). *Properties of Dry Air at One Atmosphere*. https://www.mhtlab.uwaterloo.ca/pdf_reports/mhtl_G01.pdf

[29] Peet, M. J., Hasan H. S., & Bhadeshia, H. K. D. H. (2011). Prediction of thermal conductivity of steel. *International Journal of Heat and Mass Transfer, 54*(11-12), 2602-2608. https://doi.org/10.1016/j.ijheatmasstransfer.2011.01.025

Authors' contacts:

Dalibor Videršćak, PhD, assistant
(Corresponding author)
University of Zagreb, Faculty of Mechanical Engineering and Naval Architecture,
Department of Materials,
Ivana Lučića 5, 10000 Zagreb, Croatia
dalibor.viderscak@fsb.unizg.hr

Zdravko Schauperl, PhD, Prof.
University of Zagreb, Faculty of Mechanical Engineering and Naval Architecture
Department of Materials,
Ivana Lučića 5, 10000 Zagreb, Croatia
zdravko.schauperl@fsb.unizg.hr

Sanja Šolić, PhD, Assoc. Prof.
University North, Department of Mechanical Engineering,
Jurja Križanića 31b, 42000 Varaždin, Croatia
ssolic@unin.hr

Bojan Milovanović, PhD, Assoc. Prof.
University of Zagreb, Faculty of Civil Engineering, Department of Materials,
Fra Andrije Kačića-Miošića 26, 10000 Zagreb, Croatia
bojan.milovanovic@grad.unizg.hr

Ivan Stanković, Project Coordinator
Rotarex SA,
24 rue de Diekirch, L-7440 Lintgen, Luxembourg
stankovic.ivan@rotarex.com

Mario Šercer, PhD, director
Development and Training Centre for Metal Industry Metal Centre in Čakovec,
Bana Josipa Jelačića 22D, 40 000 Čakovec, Croatia
ravnatelj@metalskajezgra.hr